International Journal of Engineering, Science and Mathematics
Vol. 6 Issue 6, October 2017,
ISSN: 2320-0294 Impact Factor: 6.765
Journal Homepage: http://www.ijesm.co.in, Email: ijesmj@gmail.com
Double-Blind Peer Reviewed Refereed Open Access International Journal - Included in the International Serial Directories Indexed & Listed at: Ulrich's Periodicals Directory ©, U.S.A., Open J-Gage as well as in Cabell's Directories of Publishing Opportunities, U.S.A

DIELECTRIC, MAGNETIC AND IMPEDANCE PROPERTIES OF BTBFT MULTI FERROIC CERAMICS

1. SHASHI PRAKASH RAI AND 2. B.K MISHARA

1.Mansa Pandey Bag, Ara – 802301 , Bihar , India

2. Shreenath Niketan , Hazaribagh-825301 , Jharkhand , India

Abstract

The ternary bulk sample of ($Bi_{0.8}Tb_{0.1}Ba_{0.1}Fe_{0.9}Ti_{0.1}O_3$)was prepared by using a solid state reaction technique. In this paper the structural, electrical and magnetic properties of ceramics have been investigated. The XRD patterns of the samples at room temperature showed perovs kite phase with hexagonal structure at room temperature. Studies of dielectric properties of the compounds with frequency at different temperatures (25-400^oC), exhibits two dielectric anomalies, one at 175^oC and other around 320^oC (ferroelectric–paraelectric type transition).The Curie temperature shifted towards the lower temperature with the increase in frequency. The low value of activation energy obtained for this ceramic samples could be attributed to the influence of electronic contribution to the conductivity. By using VSM technique, a significant change in the magnetic properties was observed for this ceramic. The highest magnetization field were found attemperature 5K. The impedance analysis confirm the non-Debye type behaviour of the compound.The relaxation frequency shifted to higher side with increase in temperature.The Nyquist plot and conductivity studies showed the NTCR character of samples.

Keywords: Ceramics; X-ray diffraction; Dielectric properties; Impedance spectroscopy; Magnetic property.

Introduction

From a technological point of view, the mutual control of electric and magnetic properties is an attractive possibility for recent research **[1]**. This offers potential applications for new devices of magnetic storage as well as ferroelectric devices. The perovskite type materials provide the vast spectrum of electrical properties covering ferroelectric-(anti-)

ferroelectric, ferromagnetic-(anti-)ferromagnetic, metallic, and semiconductor. Hence the combination of these perovs kite materials opens various routes for achieving the multi ferroism properties in one phase material. Recently, several researcher reported on the synthesis and characterization of multi ferroic perovskite systems such as anti ferromagnetic-ferroelectric, weak ferromagnetic/anti ferromagnetic-ferroelectric and antiferro magnetic/weak ferromagnetic-ferroelectric systems **[2, 3]**. As a typical ferro electromagnetic material, $BiFeO_3$(BFO) is the most useful for practical application point of view owning to its high Curie (T_C = 1103 K) and Neel (T_N = 643 K) transition temperatures, and therefore it has attracted a great deal of research interest **[4]**. Because of the canting of the Fe sub lattice moment, $BiFeO_3$ shows a weak magnetic moment at room temperature **[5]**. The spontaneous magnetic moment was absent in pure $BiFeO_3$ up to 8 kOe because of the completely compensated anti ferromagnetic ordering**[4]**. Preparation of pure $BiFeO_3$ in the bulk ceramic form without traces of impurities has been a very difficult task. $BiFeO_3$-ABO_3solid solution systems have attracted great attention as a means to increase structural stability and sinter ability. Processing of $BiFeO_3$ with other perovs kite structured materials, such as $BaTiO_3$, would prevent the formation of secondary phases **[6, 7]** and have excellent ferroelectric properties (T_C= 120^{o}C).The overall magnetic behaviors of bulk $ReFeO_3$ (Re-Rare Earth) are described as the result of two contributing magnetic 'sub lattices': (i) an anti ferromagnetic iron oxide lattice in which the spins are coupled via a Fe^{3+} - O^{2-} -Fe^{3+}super exchange mechanism; and (ii) a paramagnetic contribution from essentially non-coupled ions. Due to spin-canting in the iron containing sub lattice, a small ferromagnetic moment is observed as a result of the distorted perovs kite structure in one particular crystallographic direction**[8]**. Terbium ions (Tb^{3+}) possessing large atomic weight, smaller size (Radius Tb^{3+} = 0.923 A°) as compared to Bi^{3+} Ions (Radius Bi^{3+} = 1.032 A°), comparable electroneg ativity with respect to Bi^{3+} ions, make Tb^{3+} ions the most suitable dopant**[9-11]**. Therefore, the large structural distortions would be expected by their substitutions in $BiFeO_3$. Moreover, Tb^{3+} ions possess large magnetic moment; upon their doping, the spiral modulated spin structure of $BiFeO_3$ could be partially destroyed and the spatial homogenization of spin arrangements could be realized**[12, 13]**. This results in the enhancement of the multi ferroic properties of the $BiFeO_3$, which is the motivation for the present study.

In this study, the crystal structure, dielectric and magnetic properties of the perovskite system $Bi_{0.8}Tb_{0.1}Ba_{0.1}Fe_{0.9}Ti_{0.1}O_3$ have been carried out to examine the behavior of the ceramic system. Tb and Ba were used to substitute at the A site of $BiFeO_3$, because their radii are similar, and they stabilize the perovs kite phase that helps to decreased Bi volatilization and the amount of oxygen vacancies. This system is a combination of three ternary perovs kite (two Ferromagnetic + one Ferroelectric) systems. The origin of the weak ferromagnetism has been discussed in terms of high temperature characteristics of this perovskite system. Electrical properties have been carried out by using complex impedance and modulus spectroscopy (CIS) technique**[14]**, which is a very convenient tool to correlate the structural/microstructural and electrical properties relationship in a polycrystalline ceramics.

Material and methods

Polycrystalline samples of ($Bi_{0.8}Tb_{0.1}Ba_{0.1}Fe_{0.9}Ti_{0.1}O_3$) were synthesized from high purity oxides (Bi_2O_3 (99.9% pure M/S Aldrich chemicals USA), Fe_2O_3 (99.9% pure M/S Aldrich chemicals, USA), Tb_4O_7 (99.9% pure M/S Aldrich chemicals, USA), $BaCO_3$ (99.9% pure M/S Aldrich chemicals, USA) and TiO_2, (99.9% pure M/S Aldrich chemicals, USA), using solid-state reaction technique. The constituent compounds in suitable stoichiometric were thoroughly mixed in a ball milling unit for 42h. Then powder was dried at 125°C and calcined at 900°C for 4 h in alumina crucibles. The calcined fine powder was cold pressed into cylindrical pellets of 10 mm in diameter and 1-2 mm in thickness using a hydraulic press with a pressure of 50MPa. These pellets were sintered at a temperature i.e. 1000°C for 3 h. The formation and quality of compounds were verified with X-ray diffraction (XRD) technique. The XRD patterns of the compounds were recorded at room temperature using X-ray powder diffract to meter (Rigaku Minifiex, Japan) with CuKα radiation (λ = 1.5405 Å) in a wide range of Bragg angles 2θ ($20° \leq 2\theta \leq 60°$) at a scanning rate of 2° min^{-1}.Scanning Electron Micrographs (SEM) of the fractured surface of the specimen were obtained with a JEM-2000FX (JEOL Ltd.) scanning electron microscope operated at 25 kV.The flat polished surfaces of the sintered samples were electrode with air drying silver paste. Dielectric and impedance were determined by use of PSM1734 Impedance Analyzer at frequencies 1 kHz to 1MHz; samples were heated from room temperature to 400^0C.The magnetic data was recorded with the help of vibrating sample magnetometer (VSM) (Cryogenic).

Results and Discussion

Structural studies

Fig. 1 shows the XRD patterns of $Bi_{0.8}Tb_{0.1}Ba_{0.1}Fe_{0.9}Ti_{0.1}O_3$ ceramics at room temperature. All patterns match with JCPDS#712494 data and shows that the samples have mixed phase with a hexagonalstructure at room temperature. All the reflection peaks were indexed using observed inter-planar spacing d and lattice parameters of $Bi_{0.8}Tb_{0.1}Ba_{0.1}Fe_{0.9}Ti_{0.1}O_3$ with jcpds data base. The main peak of the samples are located at approximately $2\theta = 31.84°$, having hkl value <110>. Because of the kinetics of formation, the other impurity phases are obtained during synthesis. In my samples, the impurity phase was observed and it was shown as * in **Fig. 1** and it may be attributed to $BaFe_2O_4$ (JCPDS#772337).

SEM images of sintered ceramic samples are shown in **Fig. 2**. It was observed that the grains are homogeneously distributed over the entire surface of the samples with less porosity. The grain sizes of the ceramic are in the range of 0.5-12μm. On the other hand, from the sintered ceramic surface (as-fired), homogeneous grains of various sizes can clearly be seen.

Dielectrics studies

Fig. 3shows the variation of ε and tanδ with temperature at frequencies 1 kHz-100 kHz for $Bi_{0.8}Tb_{0.1}Ba_{0.1}Fe_{0.9}Ti_{0.1}O_3$ (BTBFT) were obtained on silver electrode samples in plane capacitor configuration. The observed peaks in the dielectric constant can be correlated to the two phase transitions from ferroelectric to ferroelectric and ferroelectric to parael ectric at temperatures 175^oC and 320^oC respectively. These two peaks are due to two different ferroelectric compounds present in the ceramic system i.e. $BiFeO_3$ and $BaTiO_3$. With increase in temperature, the dielectric constant increases up to 170^oC, and then decreases up to 235^oC. After 235^oC dielectric constant increases again up to 320^oC. This is due to the presence of different types of polarizations (electronic, atomic, ionic, dipolar and space-charge) at low frequencies and high temperatures. As in normal ferroelectrics, the dielectric constant of and samples increases gradually with increasing temperature up to the transition temperature and thereafter it decreases with increasing temperature. BTBFT sample shows the maximum value of dielectric constant with transition temperatures for different frequencies (1 kHz- 100 kHz) are shown in **Table 1.**

We observed that the real and imaginary part of dielectric constant decrease with the increase in frequencyas shown in **Fig. 4.** The decrease in the dielectric constant (ε′) can be explained on the basis of decrease in polarization with frequency. At low frequencies, all the polarizations respond easily to the time varying electric field but as the frequency of the electric field increases different polarization contributions filters out, as a result, the net polarization of the material decreases which leads to the decrease in the value of ε′. Further, the decrease of ε′′with the increase in frequency can be explained by Debye formula **[15]**. At lower frequencies tan δ is inversely proportional to frequency which explains the decrease in tanδ with frequency. $Bi_{0.8}Tb_{0.1}Ba_{0.1}Fe_{0.9}Ti_{0.1}O_3$ sample shows the maximum value of dielectric constant for different frequencies as shown in **Table 1.**

Fig. 5shows the variation of log σ_{ac} (s/m) vs 1/T (K^{-1}) of $Bi_{0.8}Tb_{0.1}Ba_{0.1}Fe_{0.9}Ti_{0.1}O_3$ ceramics at 1kHz -100 kHz frequencies in the temperature range from 325^0C to 345^0C. The ac electrical conductivity was calculated from the impedance data using the formula $\sigma = \omega\varepsilon\varepsilon_o\tan\delta$, where ε_o is the vacuum dielectric constant, ω is the angular frequency and k_B is the Boltzmann constant. The value of activation energy was calculated in the paraelectric region from the plot of $\ln(\sigma_{ac})$ vs 1/T using the conductivity relation $\sigma = \sigma_o \exp(-E_a/k_BT)$**[16]**asshown in **Table 1**.It is observed that σ_{ac} increase with increasing temperature which confirming the NTCR behaviour. At high temperature, the donor cations have a major part to play in the conduction process and activated with small energy which is called activation energy.The activation energy for all composition at different frequency was found to be very low in the paraelectric region**.** This may be due to ionic solids having a limited number of mobile ions being trapped in relatively stable potential wells during their motion through the solid. Due to a rise in temperature the donor cations are taking a major part in the conduction process. The donors have created a level (i.e. band-donor level), which is much nearer to the conduction band. Therefore, only a small amount of energy is required to activate the donors. In addition to this, a slight change in stoichiometry in multi-metal complex oxides causes the creation of large number of donors or acceptors, which creates donor or acceptors like states in the vicinity of conduction or valance bands. These donors or acceptors may also be activated with small energy**[17].**

International Journal of Engineering, Science and Mathematics
Vol. 6 Issue 6, October 2017,
ISSN: 2320-0294 Impact Factor: 6.765
Journal Homepage: http://www.ijesm.co.in, Email: ijesmj@gmail.com
Double-Blind Peer Reviewed Refereed Open Access International Journal - Included in the International Serial Directories Indexed & Listed at: Ulrich's Periodicals Directory ©, U.S.A., Open J-Gage as well as in Cabell's Directories of Publishing Opportunities, U.S.A

Electrical studies.

The electrical properties of $Bi_{0.8}Tb_{0.1}Ba_{0.1}Fe_{0.9}Ti_{0.1}O_3$ ceramics were investigated by the help of complex impedance spectroscopy (CIS) technique. It is important to transform the dielectric and electrical data in different formalism and analyze them to get true picture of the material. The use of function Z* and Y* is particularly appropriate for the resistive and/or conductive analysis where the long-range conduction dominates, whereas the ε* and M* functions are suitable when localized relaxation dominates. So the plotting of ac data in terms of impedance, electric modulus, and dielectric permittivity simultaneously gives a complete assignment of all the physical processes taking place in the material.

The variation of real part of impedance (Z′) with frequency at various temperatures (from 225 to 325 °C) for $Bi_{0.8}Tb_{0.1}Ba_{0.1}Fe_{0.9}Ti_{0.1}O_3$ ceramics is shown in **Fig. 6**. The pattern shows a sigmoid variation as a function of frequency in the low frequency region followed by a saturation region in the high frequency region. This suggests the presence of mixed nature of polarization behavior in the material, such as electronic, dipolar and orientation polarization. A decreasing trend of Z′ with rise in temperature suggests the presence of negative temperature coefficient of resistance (NTCR) in the material in the low frequency region but tends to merge in the high frequency region at almost all temperatures. A possibility of increase in ac conduction (σ_{ac}) in the sample was observed due to the decrease in the magnitude of Z′ with rise in temperature. This increase in ac conduction with temperature may be due to the contribution of defects like oxygen vacancies. Generally, the contribution due to oxygen vacancies is more prominent in perovs kite structures at higher temperatures. These results indicate increase in ac conductivity with rise in temperature in the high frequency region (possibly) due to the release of space charge and lowering in the barrier properties of the material**.**

Fig. 7 presents the variation of imaginary part of impedance (Z″) as a function of frequency at different set of temperatures (from 225 to 325 °C) for $Bi_{0.8}Tb_{0.1}Ba_{0.1}Fe_{0.9}Ti_{0.1}O_3$. With the increase of frequency, imaginary part of impedance (Z″) increases initially, attains a peak (Z''_{max}) and then decreases with frequency at all measured temperatures. At higher frequency side all the curves are merged which might be due to the reduction in space charge polarization at higher frequency. The peak shifts towards higher frequency side with increasing temperature showing that the resistance of the bulk material is decreasing. Also,

the magnitude of Z'' decreases with increasing temperature. This would imply that dielectric relaxation is temperature dependent, and there is apparently not a single relaxation time.

Fig. 8(a) shows the temperature-dependent spectra (Nyquist plot) of $Bi_{0.8}Tb_{0.1}Ba_{0.1}Fe_{0.9}Ti_{0.1}O_3$ materials. By impedance spectrum we got the semicircular arcs at the set of higher temperatures. The nature of variation of the arcs with temperature and frequency provides various clues of the materials. However, as the temperature increased the slope decreased and found to curve towards the major (Z') axis forming clear semicircular arcs. The radius of curvature was found to decrease with increasing temperature, which indicates the increase in conductivity of the sample with temperature. Generally, existence of a single semicircular arc represents only one contribution e.g. grain interior (bulk) property of the material. However, in the present case, the spectrum comprises of suppressed semicircular arcs indicating two different contributions from the grain interior (bulk) and grain boundary. The observed semicircular arcs have their centers lying off the real (Z') axis which is an indication of non-Debye type relaxation with a distribution of relaxation times instead of a single relaxation process. In general, the relaxation time for grain boundary region is much larger than that for the grains and, therefore, its response relaxes at lower frequencies. Thus, the low frequency arc in the Nyquist plot corresponds to the grain boundary effects and the smaller high frequency arc to the grain/bulk effect of the material. In the other words the semicircular arc with the real axis (Z') gives us an estimate of the bulk resistance (R_b) of the material. It has been observed that the bulk resistance of the material decreases with increase in temperature showing a typical semiconducting property, i.e. negative temperature coefficient of resistance (NTCR) behavior.The fitting of Nyquist plot for $Bi_{0.8}Tb_{0.1}Ba_{0.1}Fe_{0.9}Ti_{0.1}O_3$ ceramics shown in **Fig. 8(b)**and it observed that with the increase in temperature the slope of the lines decrease and the lines bend towards real (Z') axis and at higher temperatures (250^{o}C, 275^{o}C, 300^{o}C and 325^{o}C); a semicircle could be traced, indicating the increase in conductivity of the sample. It can also be observed that the peak maxima of the plots decrease and the frequency for the maximum shifts to higher values with the increase in temperature. It can be noticed that the complex impedance plots are not represented by full semicircle, rather the semicircular arc is depressed and the centre of the arc lies below the real (Z') axis suggesting the relaxation to be of poly dispersive non-Debye type in samples. This may be due to the presence of distributed elements in the material

electrode system.**[14, 18].** An equivalent circuit is being used to provide a complete picture of the system and establish the structural property relationship of the materials. Comparison of complex impedance plots (symbols) with fitted data (lines) using commercially available software ZSimpwin Version. To model the non-Debye response, constant phase element (CPE) is used in addition to resistors and capacitors. Here it has also been clearly observed from the Nyquist plots that the influence of grain size on the inter grain resistivity increases with decreasing grain size.

Fig.9 shows the variation of real part of electric modulus (M′) with frequency at higher temperatures between 250°C-325°Cfor $Bi_{0.8}Tb_{0.1}Ba_{0.1}Fe_{0.9}Ti_{0.1}O_3$ ceramics. It is characterized by a low value of M′ in the low frequency region followed by a continuous dispersion with increase in frequency. It was found that M′ values saturated to a maximum (M_∞ - the asymptotic value of M′ at higher frequencies) in the high frequency region for all temperatures**.** The asymmetric plot of M′ is because of the stretched exponential character of relaxation time of the material. Monotonous dispersion on increasing frequency at lower temperatures may be caused by short range mobility of charge carriers. Such results may possibly be related to a lack of restoring force governing the mobility of the charge carriers under the action of an induced electric field. The value of M′ decreases with rise in temperature in the observed frequency range.

Fig. 10 shows the variation of imaginary part of electric modulus (M″) with frequency at higher temperatures for $Bi_{0.8}Tb_{0.1}Ba_{0.1}Fe_{0.9}Ti_{0.1}O_3$ ceramics. By these graphs we found that the position of the peak M''_{max} shifted to higher frequencies as the temperature was increased. Physically, the peak in the imaginary part of the electric modulus defines the regions where the carrier can move at long distances. At frequency above peak maximum, the carriers are confined to potential wells, being mobile on short distances. The peaks are asymmetric and broader than the ideal Debye curve. Also, a peak in the M″ imaginary part indicates a dielectric relaxation process in the solid, and the frequency to the maximum indicates the mean relaxation time of this process. As can be seen, the imaginary part of the electric modulus exhibits a very well defined peak. The frequency range where the peaks occur is indicative of transition from long range to short range mobility**[19, 20].** Two peaks in graph confirms the co-existence of two systems.

International Journal of Engineering, Science and Mathematics
Vol. 6 Issue 6, October 2017,
ISSN: 2320-0294 Impact Factor: 6.765
Journal Homepage: http://www.ijesm.co.in, Email: ijesmj@gmail.com
Double-Blind Peer Reviewed Refereed Open Access International Journal - Included in the International Serial Directories Indexed & Listed at: Ulrich's Periodicals Directory ©, U.S.A., Open J-Gage as well as in Cabell's Directories of Publishing Opportunities, U.S.A

The complex electric modulus spectrum M′ versus M″ is shown in **Fig. 11**for all the samples at different temperatures. Two arcs are clearly observed over the entire measured frequency range in both the samples. In fact, the first arc is the contribution of grain boundaries whereas the second arc is the contribution of grains. The patterns are characterized by the presence of little asymmetric and depressed semicircular arcs whose centre does not lie on M′ axis. The behavior of electric modulus spectrum is suggestive of the temperature dependent hopping type of mechanism for electric conduction (charge transport) in the system and non-Debye type dielectric relaxation. In a relaxation system, one can determine the probable relaxation time (s) from the position of the loss peak in the Z″ as well as M″ vs. log f plots according to the relation: $\tau = 1/\omega = 1/2\pi f$(f is the relaxation frequency). We found that the double semicircular arcs in the complex modulus plots with a small semicircle at high frequency and a large semi-circular arc in the low frequency region at the temperatures range(300^{o}C - 375^{o}C as shown in the **Fig 11**. The modulus spectrum shows a marked change in the shape with rise in temperature suggesting a probable change in the capacitance value as a function of temperature.

Fig. 12 shows the scaling behaviour of the sample was studied by plotting the normalized plot of M''/M''_{max} and Z''/Z''_{max} as a function of the normalized frequency at different temperatures for $Bi_{0.8}Tb_{0.1}Ba_{0.1}Fe_{0.9}Ti_{0.1}O_3$ ceramics. The normalized plot overlaps on a single master curve at different temperatures. The modulus scaling behaviour gives an insight into the dielectric processes occurring inside the material **[21]**. The value of FWHM evaluated from the normalized spectrum is greater than $\log\frac{2+\sqrt{3}}{2-\sqrt{3}}$, and this indicates about non-Debye type behavior which is well supported by complex impedance plot. The peaks shifts and broadening was observed at higher frequencies with increasing temperature. The appearance of temperature dependent peaks (Z''_{max} and M''_{max}) at a characteristic frequency ($\omega_{max}=2\pi f_{max}$) indicates the presence of relaxation process, which is temperature dependent **[22]**. These relaxation processes may be due to the presence of immobile species at low temperature and defects which became mobile at high temperature.

The frequency spectra of the ac conductivity for the samples at different measuring temperatures are shown in **Fig. 13**. The frequency dependent conductivity can be described by the equation:

International Journal of Engineering, Science and Mathematics
Vol. 6 Issue 6, October 2017,
ISSN: 2320-0294 Impact Factor: 6.765
Journal Homepage: http://www.ijesm.co.in, Email: ijesmj@gmail.com
Double-Blind Peer Reviewed Refereed Open Access International Journal - Included in the International Serial Directories Indexed & Listed at: Ulrich's Periodicals Directory ©, U.S.A., Open J-Gage as well as in Cabell's Directories of Publishing Opportunities, U.S.A

$$\sigma_{ac}(\omega) = \sigma_{dc} + A\omega^{n} \quad \ldots\ldots\ldots\ldots\ldots\ldots\ldots\ldots (1)$$

Where *n* is the frequency exponent in the range of $0 < n < 1$. A and *n* are thermally activated quantities, hence electrical conduction is a thermally activated process. The frequency at which change in slope takes place is known as hopping frequency. At higher frequency, the hopping takes place by charge carriers through trap sites separated by energy barriers of varied heights. The number of charge carriers which have high relaxation time due to higher energy barriers and respond in low frequency region might be less in numbers and so the conductivity is lower at low frequencies. While the more charge carriers are with low barrier heights and these charge carriers easily respond with the frequency and at higher frequency they showed higher conductivity. The thermal energy of the charge carriers was increased at higher temperatures and so the potential height was also reduced. The conductivity spectrum shows a low frequency dispersion region followed by a high frequency plateau region. The low frequency region has been attributed to the ac-conductivity whereas the frequency independent plateau region corresponds to the dc conductivity. The dispersion behaviour may be due to presence of space charge while in the plateau region space charge vanishes. It is reasonable since the space charge vanishes at higher frequency domain. At lower temperatures σ_{ac} linearly varies with frequency and nonlinearity occurs in the high frequency region. This behaviour suggests that the hopping mechanism might be playing an important role in conduction process in the low temperature region.

Magnetic studies

Fig. 14 shows the magnetic hysteresis loops measured at 5K, 10K, 150K and 300 K. The magnetization curves of the loop at low field are not collinear and this shows a weak ferromagnetic nature of samples, which could be further confirmed by the nonzero remnant magnetization and coercivity as shown in the partly enlarged curves in the inset of **Fig. 14**. The highest magnetization, coercive field and M-H loop area were found for 5K. The enhancement of magnetization in this sample is always ascribed to the size effects of the suppression of helical order, i.e., incomplete rotation of the spins along the direction of the wave vector, increasing in spin canting due to surface strain and oxygen defects **[23, 24]**. On the other hand, oxygen defects could also enhance the magnetization by introducing Fe^{2+} into the ferromagnetic order across Fe^{3+}- O^{2-} - Fe^{2+} **[23, 25]**.Furthermore, during the high temperature annealing process, the canting angles in samples were further modulated by the

interaction between the external magnetic field and the uncompensated spins in the canted anti ferromagnetic order, which may be the major reason causing the net magnetization to increase.

The magnetic moment as a function of temperature between 5 and 300 K under zero-field cooled (ZFC) and field cooled (FC) conditions with an applied magnetic field of 0.1 T is given in**Fig. 15**. The magnetic moment (M) vs. temperature (T) curves of $Bi_{0.8}Tb_{0.1}Ba_{0.1}Fe_{0.9}Ti_{0.1}O_3$ sample under the ZFC and FC conditions present a systematic change. The high magnetization value at the lower temperature suggests the presence of uncompensated anti ferromagnetic spins (Fe^{3+})**[26]**. Initially magnetization decreases with an increase in temperature, and then increases as shown in **Fig. 15.**As temperature goes down further from 300 to 5 K, the magnetization increases rapidly, confirming that there is a magnetic phase transition. The magnetic phase transition is suggested to be a transformation of Fe sub lattice from anti- ferromagnetic to weak ferromagnetic at low temperature **[27].**The variation of M–T curves with $Bi_{0.8}Tb_{0.1}Ba_{0.1}Fe_{0.9}Ti_{0.1}O_3$ sample may be attributed to different factors like (i) variation in the oxygen stoichiometric and doping at A and B sites, (ii) reduction in particle size and (iii) change in the magnetic anisotropy**[28]**.The saturation of magnetization is not reached for all studied samples even with an applied magnetic field up to 10 T.

Conclusions

$Bi_{0.8}Tb_{0.1}Ba_{0.1}Fe_{0.9}Ti_{0.1}O_3$ (BTBFT) solid solution ceramic was prepared using solid state reaction method. BTBFT ceramics were investigated for its dielectric properties by Impedance Spectroscopy (IS) in the temperature range of RT-500^oC and in the frequency range of 100 Hz -1 MHz. Studies of temperature dependent dielectric properties of sample exhibits two dielectric anomalies one at 175^oC and other around 320^oC.Curie temperatures320^oC-310^oC and exhibiting a hexagonal crystal system and T_c decreased with frequency. In case of magnetization, the coercive field was found to be decreased with temperature 5K, 10K, 150K and 300K.A minor loop traced for all these samples indicates an anti ferromagnetic nature with weak ferromagnetism. Real and imaginary parts of complex impedance and modulus properties of the materials were investigated by using complex impedance spectroscopy (CIS) technique. At a higher temperatures, the observed double semicircles in electric modulus plots confirms about the formation of samples in single phase

and indicates the presence of both bulk and grain boundary contributions. Impedance analysis indicates the presence of mostly bulk (grain) resistive contributions in the materials at higher temperatures whereas complex modulus plots shows the presence of grains as well as grain boundary contributions in the materials. It is due to the fact that impedance plot highlights the phenomenon with largest resistance whereas electric modulus plot highlights the phenomenon with smallest capacitance. Due to the large difference between resistive values of grains and grain boundaries, it is not possible to get two semicircles on the same impedance plot. Both impedance and modulus analysis support the typical behavior of negative temperature coefficient of resistance (NTCR) of the materials. They also confirm the presence of non-Debye type of relaxation phenomenon in the materials.

References

[1] VE Wood, A Austin (1974) Austin, Possible applications for magnetoelectric materials. Int. J. Magn 5: 303.

[2] JS Kim, CI Cheon, PW Jang, YN Choi, CH Lee (2004) Ferroelectric and ferromagnetic properties of $0.2BiFeO_3$-$0.2RFeO_3$-$0.6ATiO_3$(R= Pr, Nd and A= Ba, Pb) and $0.8BiFeO_3$-$0.2BaTiO_3$. Journal of the European Ceramic Society 24: 1551.

[3] JS Kim, CI Cheon, CH Lee, PW Jang (2004) Weak ferromagnetism in the ferroelectric $BiFeO_3$–$ReFeO_3$–$BaTiO_3$ solid solutions (Re= Dy, La). Journal of applied physics 96: 468.

[4] J Wang, JB Neaton, H Zheng, et al. (2003) Epitaxial BiFeO3 Multiferroic Thin Film Heterostructures. Science 299: 1719. Doi:10.1126/science.1080615

[5] F Chang, N Zhang, F Yang, S Wang, G Song (2007) Effect of Cr substitution on the structure and electrical properties of BiFeO3 ceramics. Journal of Physics D: Applied Physics 40: 7799.

[6] M Mahesh Kumar, A Srinivas, S Suryanarayana (2000) Structure property relations in $BiFeO_3$/$BaTiO_3$ solid solutions. Journal of applied physics 87: 855.

[7] MT Buscaglia, L Mitoseriu, V Buscaglia, et al. (2006) Preparation and characterisation of the magneto-electric< i> x</i> BiFeO< sub> 3</sub>–(1−< i> x</i>) BaTiO< sub> 3</sub> ceramics. Journal of the European Ceramic Society 26: 3027.

[8] R Rai, I Bdikin, MA Valente, AL Kholkin (2010) Ferroelectric and ferromagnetic properties of Gd-doped BiFeO< sub> 3</sub>–BaTiO< sub> 3</sub> solid solution. Materials Chemistry and Physics 119: 539.

[9] R Kiyanagi, T Yamazaki, Y Sakamoto, et al. (2012) Structural and Magnetic Phase Determination of (1-x) BiFeO3–x BaTiO3 Solid Solution. Journal of the Physical Society of Japan 81(2).

[10] SO Leontsev, RE Eitel (2009) Dielectric and Piezoelectric Properties in Mn-Modified (1− x) $BiFeO_3$–x$BaTiO_3$ Ceramics. Journal of the American Ceramic Society 92: 2957.

[11] R Melgarejo, M Tomar, R Guzman, S Singh (2005) Synthesis and Structural Characterization of BiFeO3–$BaTiO_3$ Materials. Ferroelectrics 324: 101.

[12] Y-j Zhang, H-g Zhang, J-h Yin, et al. (2010) Structural and magnetic properties in Bi< sub> 1− x</sub>< i> R</i>< sub> x</sub> FeO< sub> 3</sub>(< i> x</i>= 0–1,< i> R</i>= La, Nd, Sm, Eu and Tb) polycrystalline ceramics. Journal of Magnetism and Magnetic Materials 322: 2251.

[13] J Liu, L Fang, F Zheng, S Ju, M Shen (2009) Enhancement of magnetization in Eu doped $BiFeO_3$ nanoparticles. Applied Physics Letters 95: 022511.

[14] JR Mcdonald (1987) Impedance spectroscopy: emphasizing solid materials and systems. A Wiley-Interscience Publication, John Wiley & Sons, New York.

[15] H Birey (1978) Dielectric properties of aluminum oxide films. Journal of applied physics 49: 2898.

[16] P Uniyal, KL Yadav (2009) Observation of the room temperature magnetoelectric effect in Dy doped BiFeO 3. Journal of Physics: Condensed Matter 21: 012205.

[17] L Shu, X Wei, L Jin, Y Li, H Wang, X Yao (2013) Enhanced direct flexoelectricity in paraelectric phase of Ba(Ti[sub 0.87]Sn[sub 0.13])O[sub 3] ceramics. Applied Physics Letters 102: 152904.

[18] Dk Sharma, R Kumar, R Rai, S Sharma, Al Kholkin (2012) Impedance and modulus spectroscopy characterization of sodium-bismuth titanate-based lead-free ferroelectric materials. Journal of Advanced Dielectrics 2.

[19] R Rai, I Coondoo, R Rani, I Bdikin, S Sharma, AL Kholkin (2013) Impedance spectroscopy and piezoresponse force microscopy analysis of lead-free (1−< i> x</i>)

K< sub> 0.5</sub> Na< sub> 0.5</sub> NbO< sub> 3</sub>−< i> x</i> LiNbO< sub> 3</sub> ceramics. Current Applied Physics 13: 430.

[20] A Shukla, R Choudhary, A Thakur (2009) Thermal, structural and complex impedance analysis of Mn< sup> 4+</sup> modified BaTiO< sub> 3</sub> electroceramic. Journal of Physics and Chemistry of Solids 70: 1401.

[21] P Das, P Chakraborty, B Behera, R Choudhary (2007) Electrical properties of Li< sub> 2</sub> BiV< sub> 5</sub> O< sub> 15</sub> ceramics. Physica B: Condensed Matter 395: 98.

[22] K Prasad, K Kumari, K Chandra, K Yadav, S Sen (2009) Dielectric relaxation and ac conductivity of WO3 added (Na1/2Bi1/2) TiO3 ceramic. Materials Science-Poland 27: 373.

[23] T-J Park, GC Papaefthymiou, AJ Viescas, AR Moodenbaugh, SS Wong (2007) Size-Dependent Magnetic properties of Single-Crystalline Multiferroic BiFeO3 Nanoparticles. Nano Letters 7: 766.

[24] D Kothari, VR Reddy, A Gupta, et al. (2007) Multiferroic properties of polycrystalline Bi1−xCaxFeO3. Applied Physics Letters 91.

[25] W Eerenstein, FD Morrison, J Dho, MG Blamire, JF Scott, ND Mathur (2005) Comment on "Epitaxial $BiFeO_3$ Multiferroic Thin Film Heterostructures". Science 307: 1203.

[26] I Sosnowska, TP Neumaier, E Steichele (1982) Spiral magnetic ordering in bismuth ferrite. Journal of Physics C: Solid State Physics 15: 4835.

[27] S Zhang, M Lu, D Wu, Y Chen, N Ming (2005) Larger polarization and weak ferromagnetism in quenched $BiFeO_3$ ceramics with a distorted rhombohedral crystal structure. Applied Physics Letters 87: 262907.

[28] RK Mishra, DK Pradhan, RNP Choudhary, A Banerjee (2008) Effect of yttrium on improvement of dielectric properties and magnetic switching behavior in $BiFeO_3$. Journal of Physics: Condensed Matter 20: 045218.

Figure captions:

Table 1: Details of the physical parameters of $Bi_{0.8}Tb_{0.1}Ba_{0.1}Fe_{0.9}Ti_{0.1}O_3$ ceramics.

Fig. 1. XRD patterns of the $Bi_{0.8}Tb_{0.1}Ba_{0.1}Fe_{0.9}Ti_{0.1}O_3$ceramics.

Fig. 2. SEM micrographs of surface of the $Bi_{0.8}Tb_{0.1}Ba_{0.1}Fe_{0.9}Ti_{0.1}O_3$ceramics.

Fig. 3. Variation of real part of permittivity (ε') as function of temperature of $Bi_{0.8}Tb_{0.1}Ba_{0.1}Fe_{0.9}Ti_{0.1}O_3$ceramicsat different frequencies (1kHz-100 kHz).

Fig. 4. Variation of real and imaginary part of (ε' and ε'') dielectric constant as a function of frequency of $Bi_{0.8}Tb_{0.1}Ba_{0.1}Fe_{0.9}Ti_{0.1}O_3$ceramics at different temperatures.

Fig. 5.Variation of ac conductivity ($ln\sigma_{ac}$) as a function of absolute temperature (1/T) for$Bi_{0.8}Tb_{0.1}Ba_{0.1}Fe_{0.9}Ti_{0.1}O_3$ceramics at different frequencies(1kHz-100kHz).

Fig. 6. Variation of real part of modulus (Z') with frequency at different temperatures of $Bi_{0.8}Tb_{0.1}Ba_{0.1}Fe_{0.9}Ti_{0.1}O_3$ceramics.

Fig. 7. Variation of imaginary part of modulus (Z'') with frequency at different temperatures of $Bi_{0.8}Tb_{0.1}Ba_{0.1}Fe_{0.9}Ti_{0.1}O_3$ceramics.

Fig. 8 (a)Variation of real and imaginary part (Z' and Z'') ofimpedance and (b) Fitted graph of real and imaginary part ((Z' andZ'') of impedance with different temperatures of $Bi_{0.8}Tb_{0.1}Ba_{0.1}Fe_{0.9}Ti_{0.1}O_3$ceramics.

Fig. 9. Variation of real part modulus (M') with frequency at different temperatures of $Bi_{0.8}Tb_{0.1}Ba_{0.1}Fe_{0.9}Ti_{0.1}O_3$ceramics.

Fig. 10. Variation of imaginary part modulus (M'') with frequency at different temperatures of $Bi_{0.8}Tb_{0.1}Ba_{0.1}Fe_{0.9}Ti_{0.1}O_3$ceramics.

Fig. 11. Variation of real (M') and imaginary part (M'') of modulus with different temperatures of $Bi_{0.8}Tb_{0.1}Ba_{0.1}Fe_{0.9}Ti_{0.1}O_3$ceramics.

Fig. 12. Scaling behavior of (Z''/Z'_{max}) and (M''/M''_{max}) vs. log (f/f_{max}) of $Bi_{0.8}Tb_{0.1}Ba_{0.1}Fe_{0.9}Ti_{0.1}O_3$ceramics.

Fig. 13. Variation of $ln\sigma_{ac}$ (Ω/cm^{-1}) vs. frequency of $Bi_{0.8}Tb_{0.1}Ba_{0.1}Fe_{0.9}Ti_{0.1}O_3$ ceramics at different temperatures.

Fig.14. M–H loops of $Bi_{0.8}Tb_{0.1}Ba_{0.1}Fe_{0.9}Ti_{0.1}O_3$ceramics at (a) 5K, 10Kand(b) 150K, 300 K.

Fig.15. Variation of magnetic moment with temperature of $Bi_{0.8}Tb_{0.1}Ba_{0.1}Fe_{0.9}Ti_{0.1}O_3$ceramics for FC and ZFC.

Table 1: Details of the physical parameters of $Bi_{0.8}Tb_{0.1}Ba_{0.1}Fe_{0.9}Ti_{0.1}O_3$ ceramics.						
Sample Name	***Freq.***	$T_{FE\text{-}FE}(^oC)$	ε_{max} ***(FE-FE)***	$T_{FE\text{-}PE}(^oC)$	ε_{max} ***(FE-PE)***	E_a *(eV)*
$Bi_{0.8}Tb_{0.1}Ba_{0.1}Fe_{0.9}Ti_{0.1}O_3$	*1kHz*	*175*	*7298*	*315*	*2338*	*1.46*
	10kHz	*170*	*2101*	*320*	*920*	*1.37*
	100kHz	*170*	*722*	*310*	*384.5*	*1.06*

International Journal of Engineering, Science and Mathematics
Vol. 6 Issue 6, October 2017,
ISSN: 2320-0294 Impact Factor: 6.765
Journal Homepage: http://www.ijesm.co.in, Email: ijesmj@gmail.com
Double-Blind Peer Reviewed Refereed Open Access International Journal - Included in the International Serial Directories Indexed & Listed at: Ulrich's Periodicals Directory ©, U.S.A., Open J-Gage as well as in Cabell's Directories of Publishing Opportunities, U.S.A

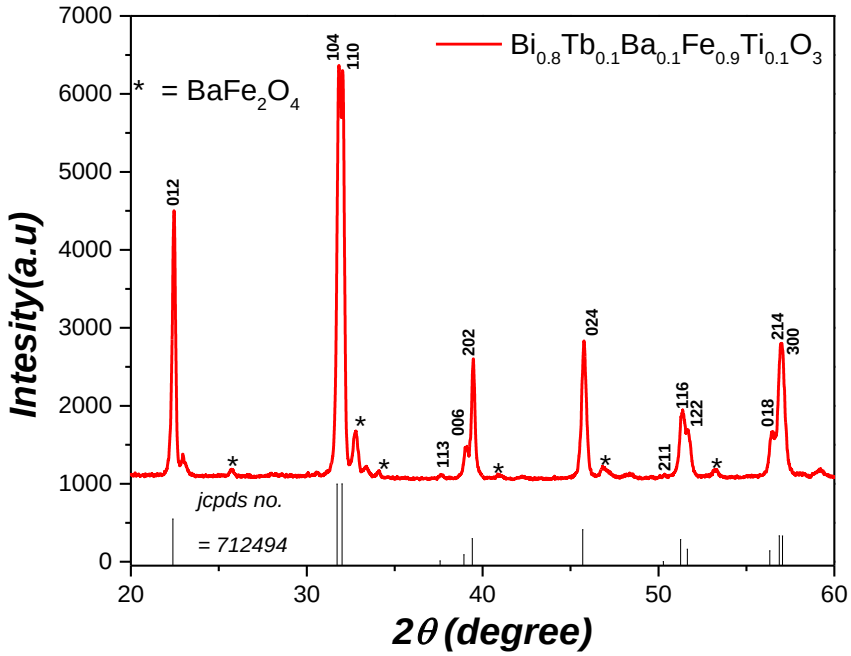

Fig. 1. XRD patterns of the $Bi_{0.8}Tb_{0.1}Ba_{0.1}Fe_{0.9}Ti_{0.1}O_3$ceramics.

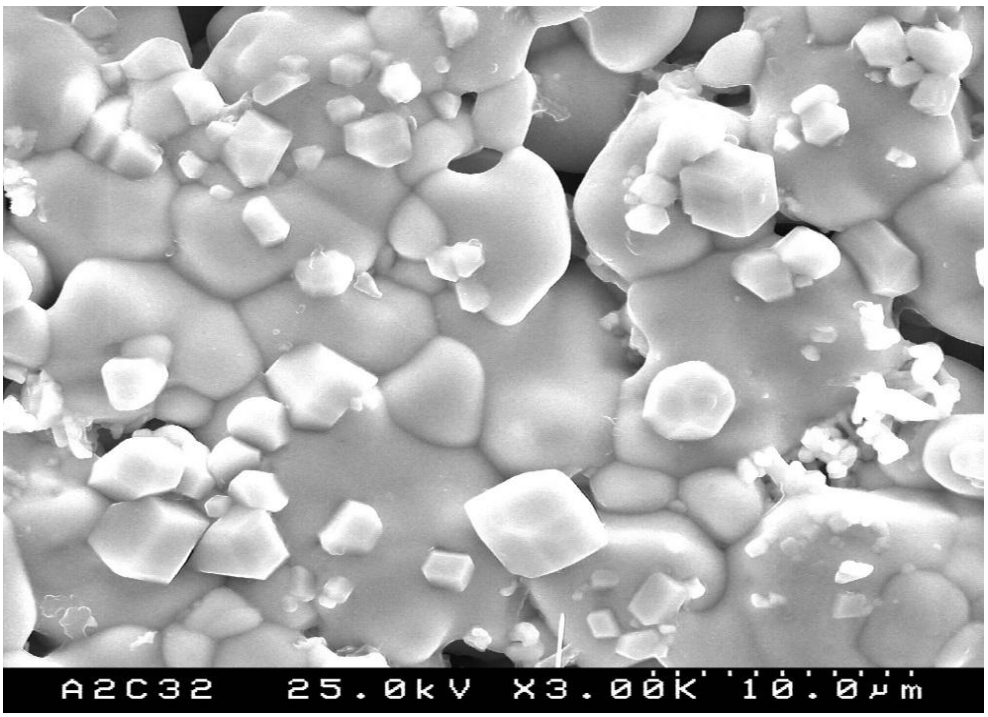

Fig. 2. SEM micrographs of surface of the $Bi_{0.8}Tb_{0.1}Ba_{0.1}Fe_{0.9}Ti_{0.1}O_3$ceramics.

International Journal of Engineering, Science and Mathematics
Vol. 6 Issue 6, October 2017,
ISSN: 2320-0294 Impact Factor: 6.765
Journal Homepage: http://www.ijesm.co.in, Email: ijesmj@gmail.com
Double-Blind Peer Reviewed Refereed Open Access International Journal - Included in the International Serial Directories Indexed & Listed at: Ulrich's Periodicals Directory ©, U.S.A., Open J-Gage as well as in Cabell's Directories of Publishing Opportunities, U.S.A

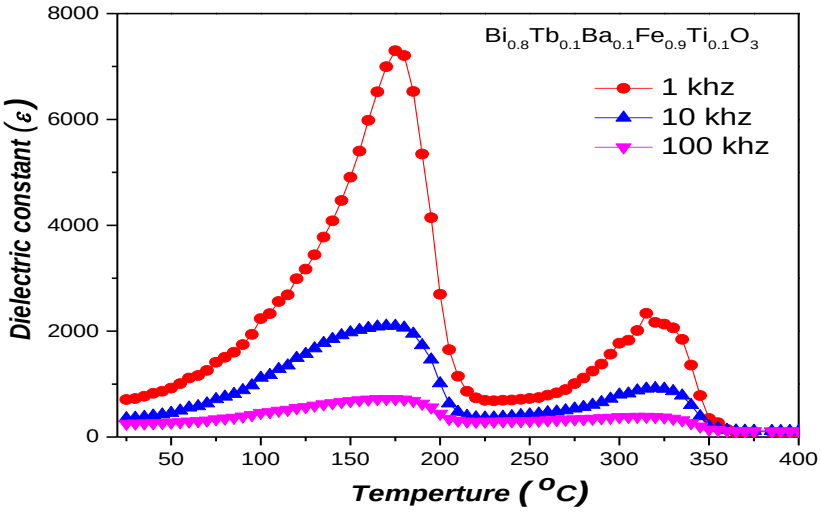

Fig. 3. Variation of dielectric constant (ε′) as function of temperature of $Bi_{0.8}Tb_{0.1}Ba_{0.1}Fe_{0.9}Ti_{0.1}O_3$ceramicsatdifferent frequencies (1kHz-100kHz).

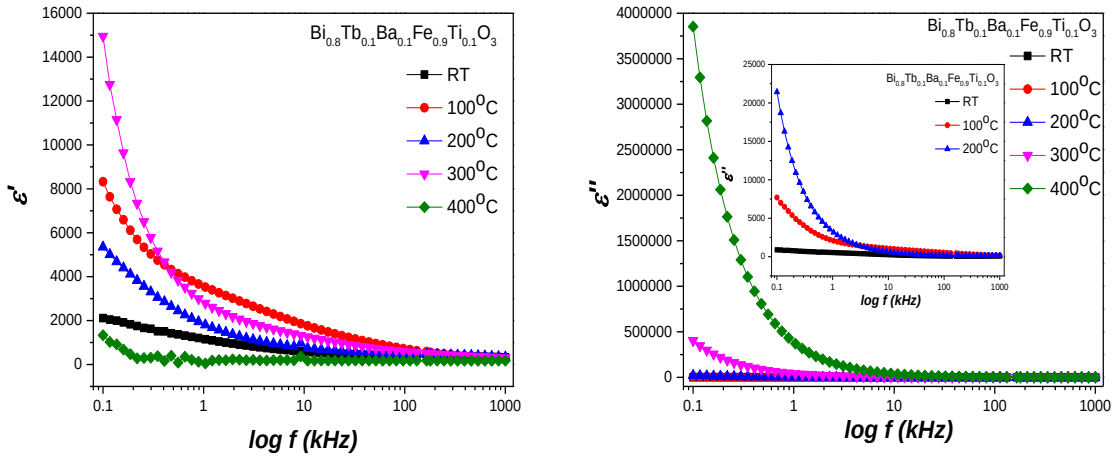

Fig. 4. Variation of real and imaginary part of (ε′ and ε″) dielectric constant as a function of frequency of $Bi_{0.8}Tb_{0.1}Ba_{0.1}Fe_{0.9}Ti_{0.1}O_3$ceramics at different temperatures.

International Journal of Engineering, Science and Mathematics
Vol. 6 Issue 6, October 2017,
ISSN: 2320-0294 Impact Factor: 6.765
Journal Homepage: http://www.ijesm.co.in, Email: ijesmj@gmail.com
Double-Blind Peer Reviewed Refereed Open Access International Journal - Included in the International Serial Directories Indexed & Listed at: Ulrich's Periodicals Directory ©, U.S.A., Open J-Gage as well as in Cabell's Directories of Publishing Opportunities, U.S.A

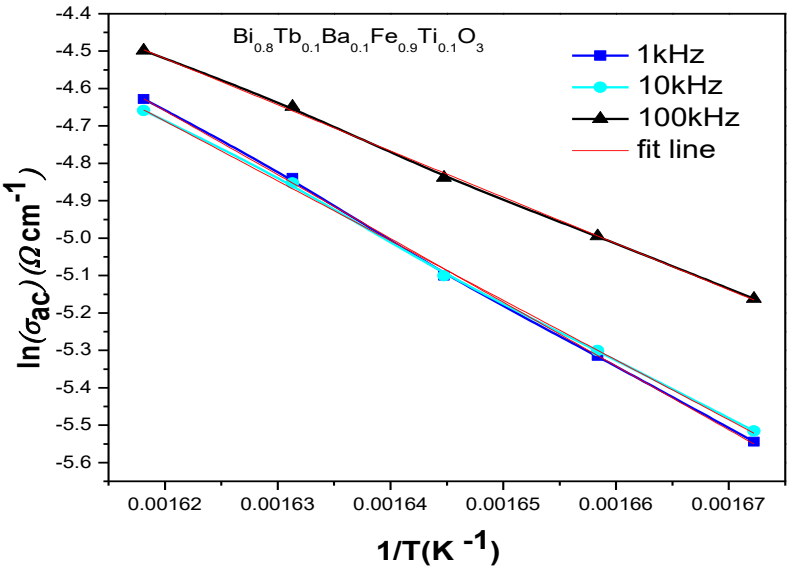

Fig. 5. Variation of ac conductivity ($ln\sigma_{ac}$) as a function of absolute temperature (1/T) for$Bi_{0.8}Tb_{0.1}Ba_{0.1}Fe_{0.9}Ti_{0.1}O_3$ ceramics at different frequencies (1kHz-100kHz).

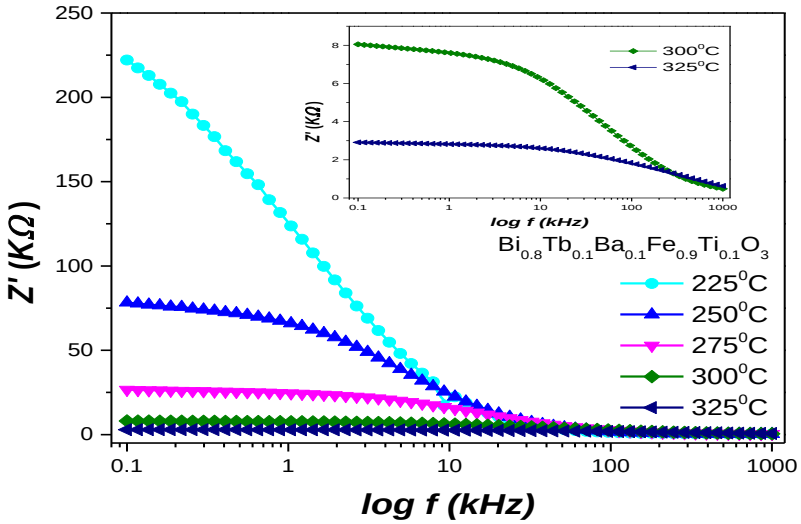

Fig. 6. Variation of real part of modulus (Z') with frequency at different temperatures of $Bi_{0.8}Tb_{0.1}Ba_{0.1}Fe_{0.9}Ti_{0.1}O_3$ceramics.

International Journal of Engineering, Science and Mathematics
Vol. 6 Issue 6, October 2017,
ISSN: 2320-0294 Impact Factor: 6.765
Journal Homepage: http://www.ijesm.co.in, Email: ijesmj@gmail.com
Double-Blind Peer Reviewed Refereed Open Access International Journal - Included in the International Serial Directories Indexed & Listed at: Ulrich's Periodicals Directory ©, U.S.A., Open J-Gage as well as in Cabell's Directories of Publishing Opportunities, U.S.A

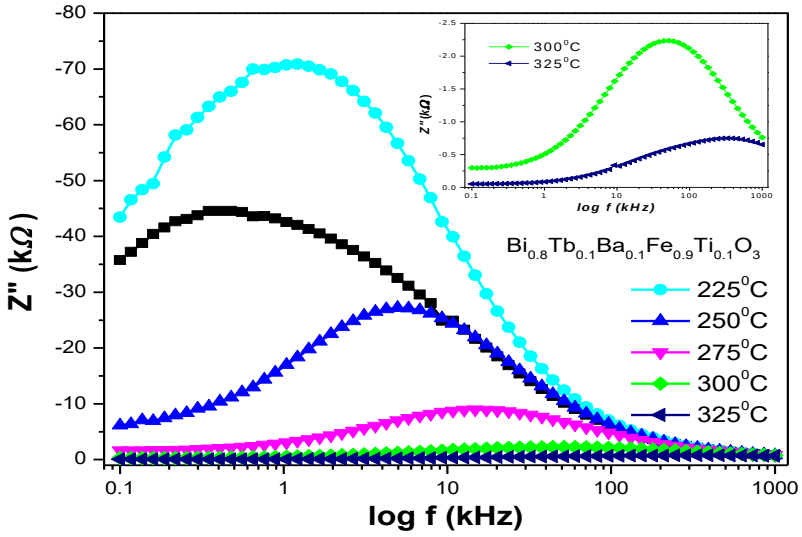

Fig. 7. Variation of imaginary part of modulus (Z'') with frequency at different temperatures of $Bi_{0.8}Tb_{0.1}Ba_{0.1}Fe_{0.9}Ti_{0.1}O_3$ceramics.

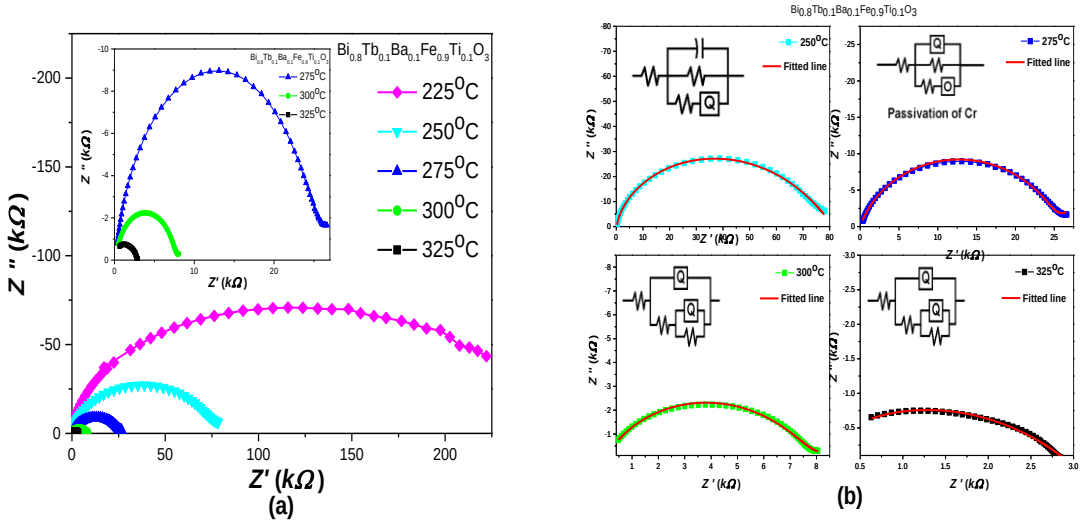

Fig. 8. (a)Variation of real and imaginary part (Z' and Z'') ofimpedanceand (b) Fitted graph of real and imaginary part ((Z' andZ'') of impedance with different temperatures of $Bi_{0.8}Tb_{0.1}Ba_{0.1}Fe_{0.9}Ti_{0.1}O_3$ceramics.

International Journal of Engineering, Science and Mathematics
Vol. 6 Issue 6, October 2017,
ISSN: 2320-0294 Impact Factor: 6.765
Journal Homepage: http://www.ijesm.co.in, Email: ijesmj@gmail.com
Double-Blind Peer Reviewed Refereed Open Access International Journal - Included in the International Serial Directories Indexed & Listed at: Ulrich's Periodicals Directory ©, U.S.A., Open J-Gage as well as in Cabell's Directories of Publishing Opportunities, U.S.A

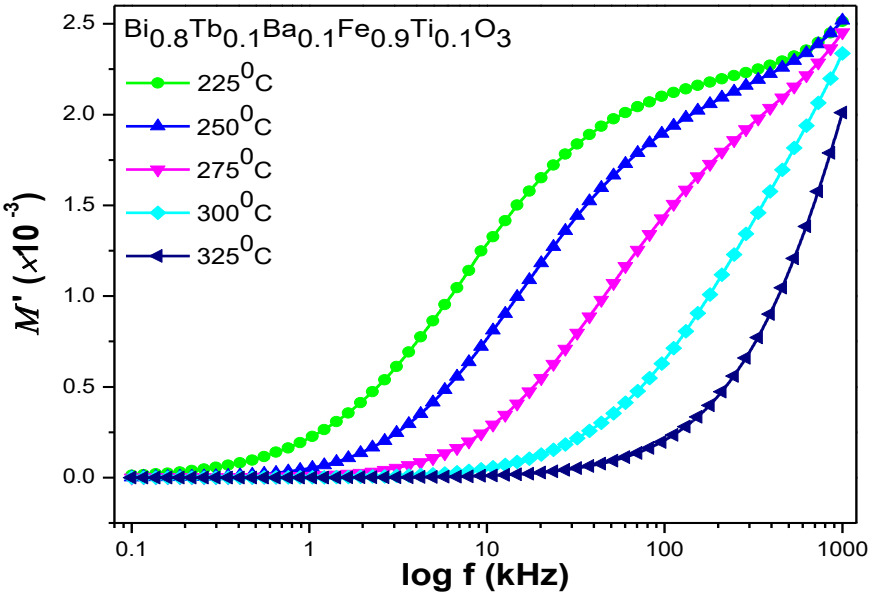

Fig. 9. Variation of real part modulus (M') with frequency at different temperatures of $Bi_{0.8}Tb_{0.1}Ba_{0.1}Fe_{0.9}Ti_{0.1}O_3$ceramics.

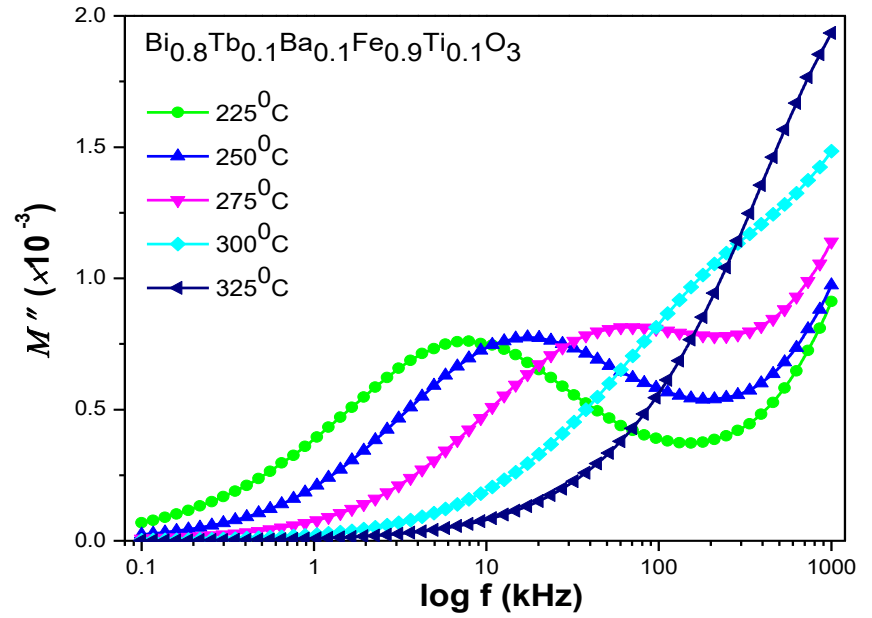

Fig. 10. Variation of imaginary part modulus (M'') with frequency at different temperatures of $Bi_{0.8}Tb_{0.1}Ba_{0.1}Fe_{0.9}Ti_{0.1}O_3$ceramics.

International Journal of Engineering, Science and Mathematics
Vol. 6 Issue 6, October 2017,
ISSN: 2320-0294 Impact Factor: 6.765
Journal Homepage: http://www.ijesm.co.in, Email: ijesmj@gmail.com
Double-Blind Peer Reviewed Refereed Open Access International Journal - Included in the International Serial Directories Indexed & Listed at: Ulrich's Periodicals Directory ©, U.S.A., Open J-Gage as well as in Cabell's Directories of Publishing Opportunities, U.S.A

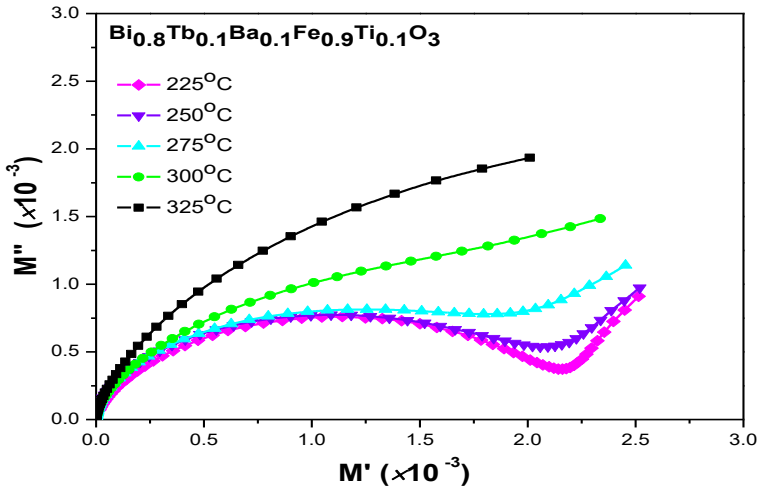

Fig. 11. Variation of real (M') and imaginary part (M'') of modulus with different temperatures of $Bi_{0.8}Tb_{0.1}Ba_{0.1}Fe_{0.9}Ti_{0.1}O_3$ceramics.

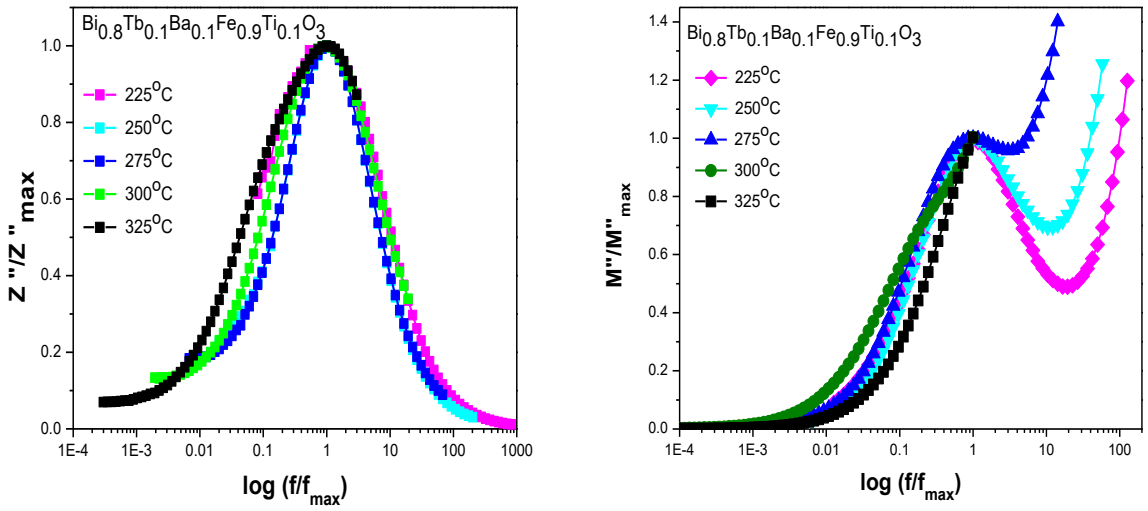

(a) (b)

Fig. 12. Scaling behavior of (Z'' / Z''_{max}) and (M'' / M''_{max}) vs log (f/f_{max}) of $Bi_{0.8}Tb_{0.1}Ba_{0.1}Fe_{0.9}Ti_{0.1}O_3$ceramics.

International Journal of Engineering, Science and Mathematics
Vol. 6 Issue 6, October 2017,
ISSN: 2320-0294 Impact Factor: 6.765
Journal Homepage: http://www.ijesm.co.in, Email: ijesmj@gmail.com
Double-Blind Peer Reviewed Refereed Open Access International Journal - Included in the International Serial Directories Indexed & Listed at: Ulrich's Periodicals Directory ©, U.S.A., Open J-Gage as well as in Cabell's Directories of Publishing Opportunities, U.S.A

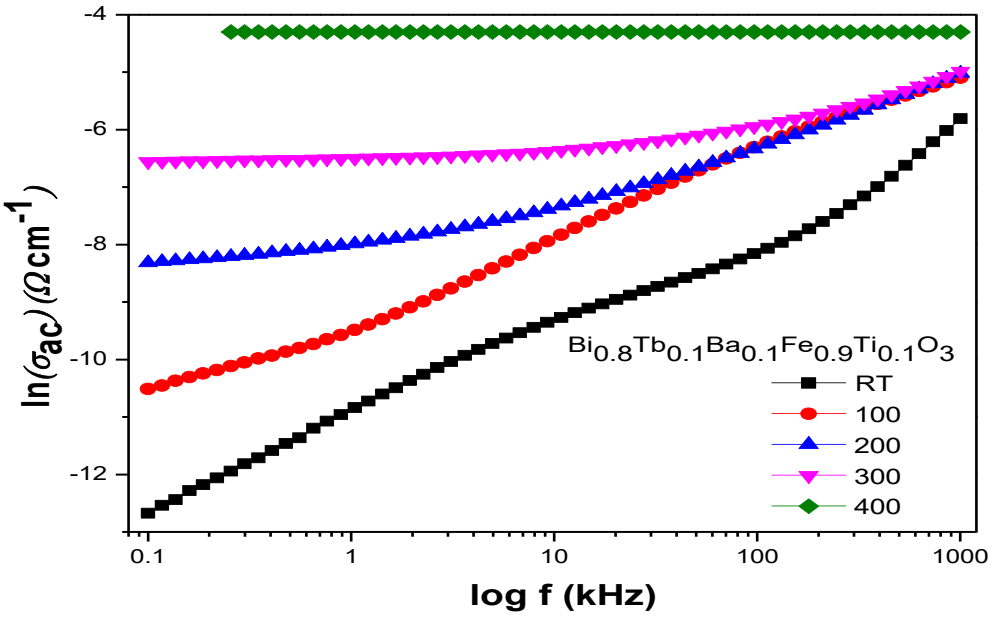

Fig. 13. Variation of $ln\sigma_{ac}$ (Ω/cm^{-1}) vs. frequency of $Bi_{0.8}Tb_{0.1}Ba_{0.1}Fe_{0.9}Ti_{0.1}O_3$ ceramics at different temperatures.

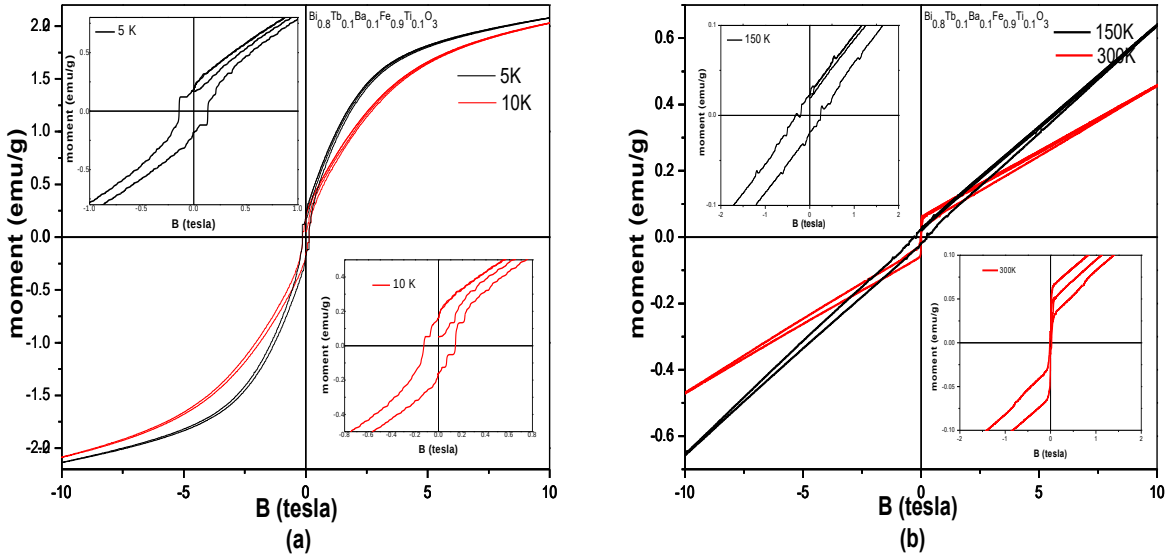

Fig.14. M–H loops of $Bi_{0.8}Tb_{0.1}Ba_{0.1}Fe_{0.9}Ti_{0.1}O_3$ceramics at (a)5K, 10K and(b)150K, 300K.

International Journal of Engineering, Science and Mathematics
Vol. 6 Issue 6, October 2017,
ISSN: 2320-0294 Impact Factor: 6.765
Journal Homepage: http://www.ijesm.co.in, Email: ijesmj@gmail.com
Double-Blind Peer Reviewed Refereed Open Access International Journal - Included in the International Serial Directories Indexed & Listed at: Ulrich's Periodicals Directory ©, U.S.A., Open J-Gage as well as in Cabell's Directories of Publishing Opportunities, U.S.A

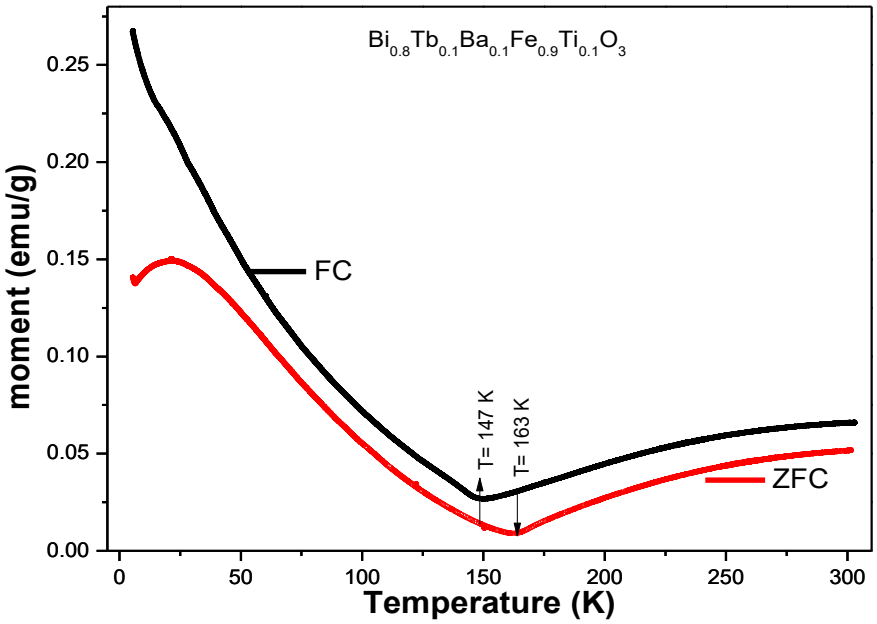

Fig.15.Variation of magnetic moment with temperature of $Bi_{0.8}Tb_{0.1}Ba_{0.1}Fe_{0.9}Ti_{0.1}O_3$ceramics for FC and ZFC.